



Application of Remote Sensing and Spectroradiometry in Geological Mapping: a case study of Handeni (QDS 148) Block, Eastern Mozambique Belt, Tanzania

Masota M Magigita^{1,2}, Elisante Mshiu², Cassy Mtelela²

¹ Geological Survey of Tanzania, P.O. Box 903, Dodoma, Tanzania

² Department of Geosciences, University of Dar es Salaam, P.O. Box 35052, Dar es Salaam, Tanzania

Corresponding author: mshiutz@gmail.com / magigita@gmail.com

Co-authors' email addresses: mshiutz@gmail.com; cassy.mtelela@gmail.com

Received 20 Jul 2023, Revised 30 Oct 2023, Accepted Nov 2023, Published Jan 2024

<https://dx.doi.org/10.4314/tjs.v49i5.12>

Abstract

This study applies remote sensing (RS) as a geologic mapping aid tool, using Handeni Block of Tanzania as a case study. To achieve the objective of this study, we have utilized various RS processing and image enhancement techniques on multispectral data, including ASTER, Landsat 5, Landsat 8, and Sentinel 2A. The method proved successful whereby both Landsat-5-data with band combination (BC) 7:4:2 and 7:5:4 and band ratio (BR) 5/3:5/1:7/5 and Landsat-8 data with BCs 5:6:7 and 7:6:4 mapped out marble units. Sentinel 2A data (with BC 8:11:3, BRs 12/2:11/2:8/11; 12/4:11/3:11/2 and 12/4:12/2:11/3) together with image enhancement decorrelation stretch on BC 4:3:2 and BC 8:11:3 images succeeded to map other major geologic units. The findings were tested using another approach, an unsupervised classification (K-means algorithm) of Landsat 8 data and unsupervised and supervised classifications by IsoData and minimum distance algorithms, respectively. Similar results were obtained from the image classification whereby Sentinel 2A data produced classified images, which consistently delineate the same lithologies. Geologic structures (lineaments) have been mapped by ASTER DEM data. The result from supervised classification using end-member spectra of the collected representative rock samples also supports the remotely sensed lithologies, demonstrating the usefulness of RS in geologic mapping. The finding of this work have shown that the integration of RS and rock spectral analyses can be used as a robust aiding tool in geologic mapping. The method is more resource efficient than a purely conventional approach.

Keywords: multispectral data, spectra profile, Handeni Block, quarter degree sheet, remote sensing (RS).

Introduction

Geologic mapping is essential in exploring the earth's resources such as minerals, water, oil, and natural gas (Gandhi and Sarkar 2016). The information gathered during geological mapping is used to prepare geological maps (Soller 2004), which traditionally display the distribution of lithologies, structures and the relative timing of formation of different rock units across the mapped area. Information

obtained from geologic mapping (and geologic maps) are used in the exploration of Earth resources, monitoring geologic hazards, land-use planning, and in construction engineering (Bhagwat and Ipe 2000).

Geological mapping has, for decades, been conducted by conventional method that involve physical fieldwork and documentation (Gandhi and Sarkar 2016), an approach that is considered expensive in a sense that a lot of

finance, human and time resources are involved (Gandhi and Sarkar 2016). Field geological mapping is also challenging when the area to be mapped is practically remote or falls in reserved areas such as games and natural forests. Consequently, geologists devise alternative approaches to supplement field geologic mapping, including geophysical methods such as radiometric and magnetic surveys (Moses et al. 2015).

Advancement in technology over the last three decades has enabled remote sensing (RS) technology to be applied in various monitoring of the Earth surfaces like in oil-slick analysis and reef in sea areas as well as in land use planning (e.g., Chunming Wu et al. 2018, Saibi et al. 2018). RS has also evolved into a valuable tool to supplement conventional geological mapping (e.g., Bhan and Krishnanunni 1983, Saibi et al. 2018). The RS technology uses the characteristic effects/responses of the Earth's geological features to the incoming electromagnetic radiation, recorded by specific atmospheric sensors; and uses satellite data collected from large areas, including those that are conventionally inaccessible.

In Tanzania, about 5 per-cents of the total area have not been mapped (GST 2018), and a large portion of the remaining 95 per-cent is not mapped at a detailed scale. Most of the available geologic maps were produced during regional field-based geological, geochemical, and airborne geophysical surveys conducted in 1930 -1970s. As such, the maps are old and likely missing much information based on existing technology. Subsequently, these maps warrant an update (*sensus* Gandhi and Sarkar 2016, and the unpublished GST Progress Map 2018). However, the country (Tanzania) is divided into 322 quarter-degree sheets (QDSs) blocks of nearly 3000 square km each. Mapping one QDS block costs about 80 to 100 million Tanzania shillings. With the available financial resources at the national geological survey (GST), only 2 to 3 QDS blocks can be mapped annually. Thus, a follow-up country-wide geological mapping will require over 50 years. Ultimately, it is crucial to apply modern technology, particularly remote sensing, to aid

in geological mapping at regional and small scales in Tanzania to produce timely outputs that match the present-day demands.

As a tool in mapping, the RS technology has rarely been used in regional geological mapping in Tanzania (e.g., Mshiu 2011). The technology has been applied in other fields, such as mapping vegetation species, land use, and monitoring volcanic activities at the Oldoinyo Lengai (e.g., Maswi and Mshiu 2020). The RS technology has been demonstrated to be an essential aid in geologic mapping in other countries (e.g., Abdeen et al. 2001, Yajima et al. 2009, Ali and Pour 2014, Fal et al. 2018).

Besides the earlier (1960s-1970s) regional geologic mapping, the Handeni (QDS 148) Block was also recently mapped by the Geological Survey of Tanzania in 2005 and by Moses et al. (2015). The two versions of the geologic maps (Figure 2) differs significantly due to difference in the data type used for compilation. Motivated by the argue to resolve this and, generally to test application of the integration of RS and rock spectral analyses, this study was set to use Handeni Block as a case study to remote-sensing-aided geologic mapping in Tanzania. Indeed, the findings demonstrate how effective and efficient this novel approach can be in geologic mapping.

Geologic Setting of Handeni (QDS 148) Block

The Handeni (QDS 148) Block occurs within the Pan African Mozambique Orogenic Belt in the eastern Tanzania, bounded to the west by the Archean Tanzanian craton (Figure 1). The Handeni (QDS 148) Block is characterized by igneous and metamorphic rocks and sedimentary rocks (Solesbury 1964, Chao 1974: Figure 2a). In a more detailed manner, the geology of Handen is described in two-fold classification: i) Neoproterozoic supracrustal felsic to mafic and ultramafic metamorphic rock assemblage of - quartz-feldspar-biotite gneiss, biotite-hornblende-feldspar gneiss, migmatitic biotite-bearing quartzofeldspathic gneiss, metapelitic gneiss/schist; and ii) the Plutonic rock category of garnet amphibolite, intermediate gneissic granulite, mafic granulite,

serpentinite, gabbro- metagabbro, pyroxenite, charnockite, migmatitic granitic orthogneiss, tonalitic orthogneiss, meta-anorthosite complex, gneissic garnet granulite, quartz

feldspathoid granulitic gneiss and marble (Moses et al. 2015: Figure 2b).

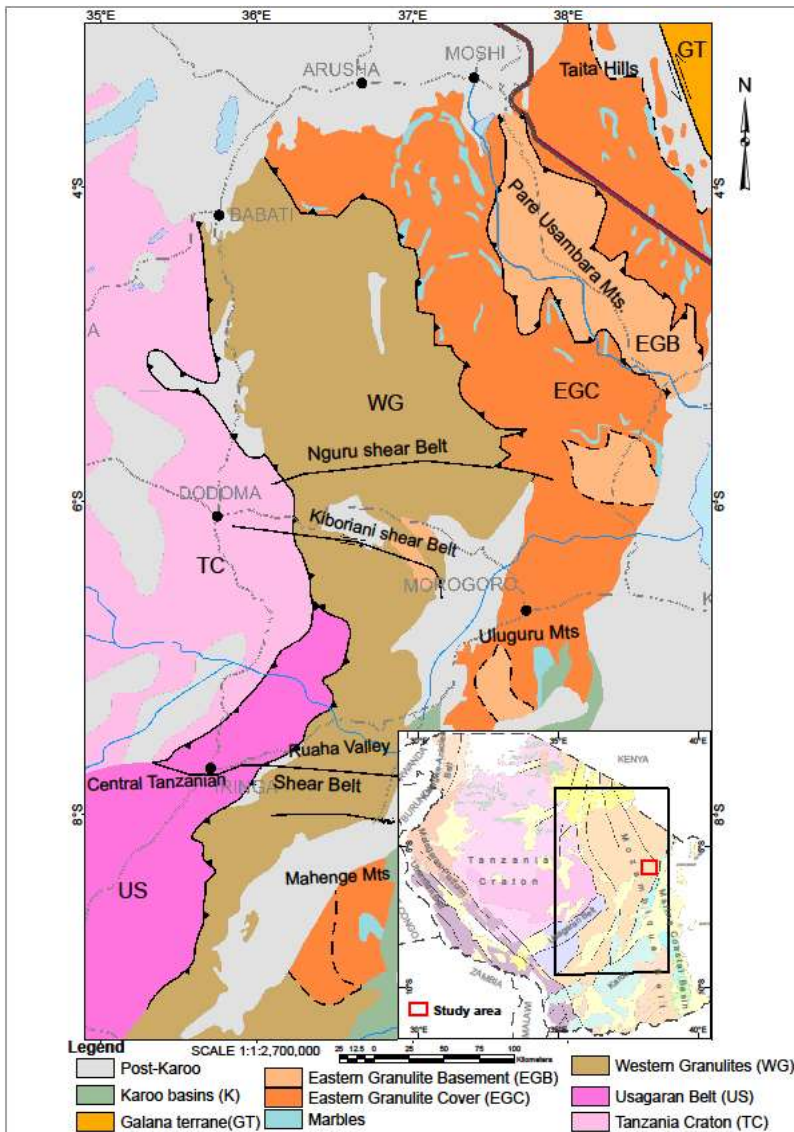


Figure 1: Overview geologic map of the eastern Mozambique Belt with an insert, showing location of the study area, modified from Fritz et al. 2009 and Leger et al. 2015. Note TC = Tanzania Craton, US = Usagarani Belt, WG = Western Granulites, EGC = Eastern Granulite Cover, and EGB = Eastern Granulite Basement.

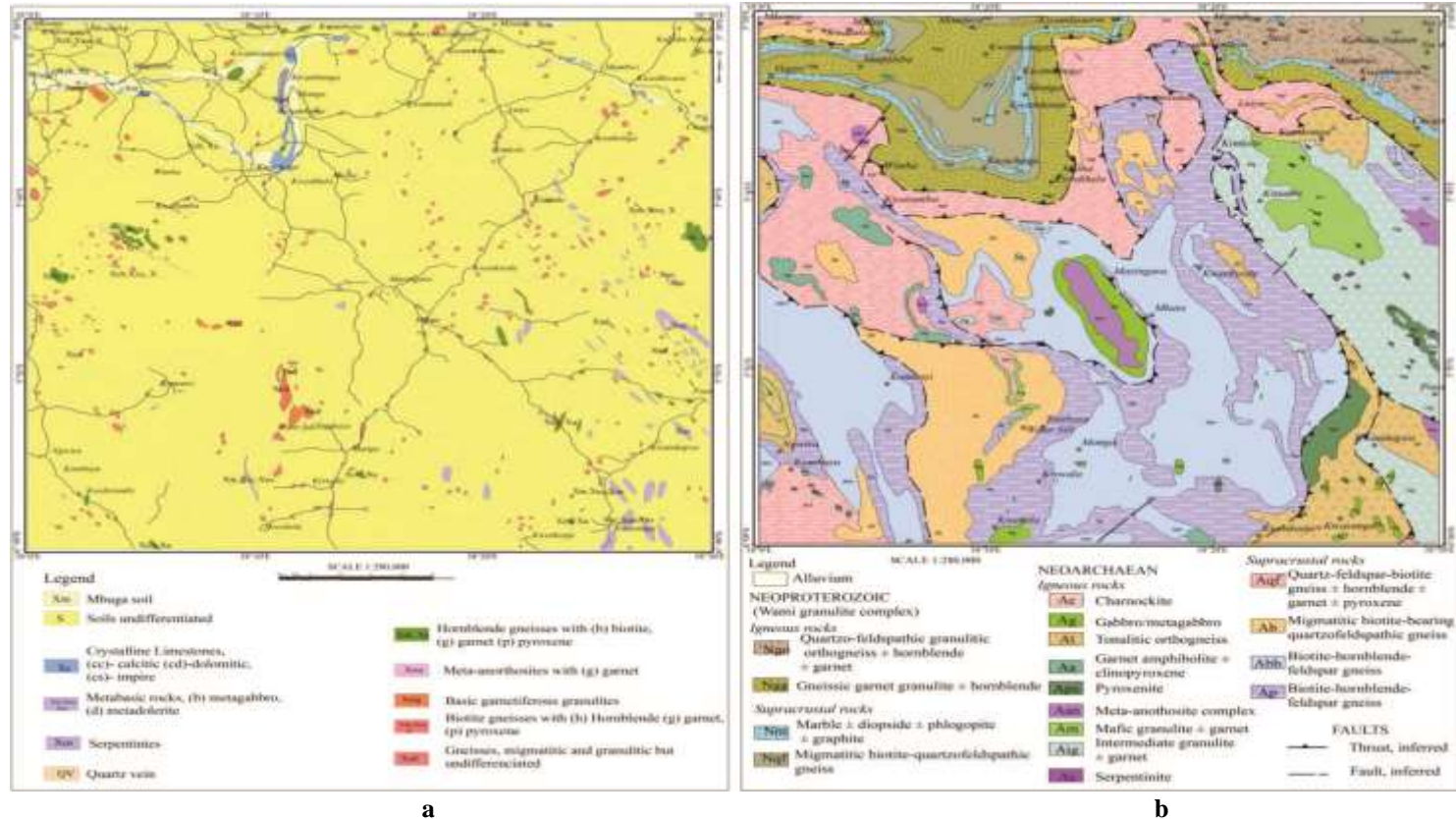


Figure 2: Two version of geological maps of Handeni (QDS 148) Block: (left) map describing surface geological units and structures (modified after Solesbury (1964) and Chao (1974); and (right) Subsurface geological map showing different lithologies and major structures (Moses et al. 2015).

The Handeni (QDS 148) Block has a complex structural trend resulting from multiple tectonic deformation events. The major regional structures trends dominantly in the southwest direction (Solesbury 1964). Most of the area is dominated by a large synform with a northern recumbent limb with lineation's striking NW-SE, plunging SE. Few minor folding has been observed in road cuttings (Solesbury 1964). Chao (1974) reported that the regional foliation trend is NW-SE to N-S while the dipping is towards the NE-E and SW directions, respectively. To the south of this structure, the strata generally strike NW and dip moderately towards the east. However, dip reversals are common, which indicates tight isoclinal folding along a NW trending axis. North-northwest trending graphitic shears and east-northeast trending faults have also been mapped in drill cores and the outcrops found in Magambazi (Archibald 2013).

Materials and Methods

Fieldwork, Spectral, and Mineral Analyses

Rock samples from pre-selected areas were collected for laboratory spectral and petrographic analyses. Rock spectral signatures from rock samples were collected at the University of Dar-es-Salaam laboratory (Tanzania) by using ASD FieldSpec Hi-Res spectroradiometer in the spectrum of visible near-infrared (VNIR) to short wave infrared (SWIR). Resultant average spectral profiles were resampled to multispectral data and to US Geological Survey (USGS) mineral spectral library to compare them with spectral profiles of known minerals from the USGS mineral spectral library as presented by Rao et al. 2017. Spectral analyst in ENVI 4.7 software was used to identify rock-forming

Sentinel 2A Data Processing Techniques

Sentinel-2A data are high-resolution data that can be acquired from European Space Agency (ESA). Two Sentinel 2A images acquired on 2016/10/08 used in the study were freely downloaded from the US Geological Survey (USGS) website <https://glovis.usgs.gov/>. The Sentinel 2A images are:

i) S2A_OPER_MSI_L1C_TL_MTI_20161008T112131_A006767_T37MCP (0.1088% clouds); and ii) S2A_OPER_MSI_L1C_TL_MTI_20161008T112131_A006767_T37MDP (0.7318% clouds). Bands 2, 3, 4, 6, 8, 8A, 11 & 12 were used, while bands 1, 5, 7, 9, and 10 were not used in the study). Sentinel 2A data processing techniques are summarised in Tables 1 - 3.

minerals of rock samples by matching rock spectral profiles with spectral profiles from USGS mineral spectral library by using Spectral Angle Mapper (SAM) and Spectral Feature Fitting (SFF) algorithms. The averaged rock samples spectra were resampled to Sentinel 2A data and produced classified image used for geologic mapping in the study area. Six rock samples were sent to the laboratory for petrographic analysis. Eleven (11) representative rock samples were analyzed by X-Ray Diffraction (XRD) for their mineral content. Furthermore, collected rock spectra were analyzed in the Spectral Geologist (TSG) software to measure and estimate the weight percentage of major composing minerals of their respective rocks.

Multispectral Data Acquisition and Pre-processing Techniques

Free downloaded acquired multispectral data processed and analyzed in this work are ASTER, Landsat 5, Landsat 8, Sentinel 2A, ASTER-DEM, and high-resolution airborne geophysical data. The acquired data (images) were ortho and geometric corrected to remove the image production errors and noises, to enhance the processing and interpretation of the images for lithological and structure mapping. The downloaded images were pre-processed to remove unwanted pixels (masking) to interpret geological signatures. Then various processing and enhancement techniques were applied to the images to enhance the lithological discrimination of the surface geology. Raw satellite data were processed and images were overlaid with other available data by (QGIS) 3.2.2, ENVI 4.7, ArcMap 10.3, and ERDAS software.

ASTER Data Processing Techniques

The Advanced Spaceborne Thermal Emission and Reflection Radiometer (ASTER) is a high-resolution multispectral remote sensing sensor (e.g., Pour et al. 2015). Three L1T ASTER scenes were freely downloaded from the USGS Earth Explorer website. The ASTER data were identified as:

- i) AST_L1T_00311302003075027_20150502061719_48606-(2/05/2015).
- ii) AST_L1T_00302172007075558_20150518075516_61226-(18/05/2015).
- iii) AST_L1T_00302172007075549_20150518075509_21935-(27/01/2006).

The ASTER Data processing techniques are summarized in Tables 1 - 3.

Landsat 5 and 8 Data Processing Techniques

Two Landsat 8 (OLI) data scenes and one Landsat TM5 scene used for this study were downloaded from the USGS's websites, <http://earthexplorer.usgs.gov> and <http://glovis.usgs.gov/>. The data are listed below:-

- i) LC08_L1TP_167064_20150114_20170414_01_T1 with cloud coverage of 9.44%.
- ii) LC08_L1TP_167064_20170916_20170929_01_T1 with cloud coverage of 1.92%.
- iii) LT05_L1TP_167064_20050219_20161127_01_T1 with 0% cloud coverage.

Two Landsat 8 data scenes of 2015 (b1) and 2017 (b2) were then fused by image band math "(b1 le 0)* b2 OR (b1 ge 0)*b1" in ENVI software to increase the image information pixels which have been masked out in each scene during pre-processing. The processing techniques for these data are also summarised in Tables 1 - 3.

ASTER Dem and SRTM Processing Techniques

ASTER Digital Elevation Model (ASTGTM) data was also used with the shuttle radar topographic mission (SRTM) data. ASTGTM and SRTM data have 30- and 90-meters spatial resolution, respectively. The Aster DEM data are available for free download on the [link](#)

<https://earthexplorer.usgs.gov/>. The data are obtained with a projection of the Universal Transverse Mercator (UTM) and a World Geodetic System WGS 84 datum (Mshiu 2011). Tables 1 - 3 of the summarise all image processing and enhancement techniques used during the research.

Table 1: Multispectral data processing with different band combinations (BC) tested in this study.

Satellite Data	Band Combinations	Target/lithology	References
Landsat 8 (OLI) OLI 8 (2017) OLI 8 (2015)	7:5:3, 7:6:4, 6:7:4, 5:6:7, 6:5:2, 1:6:7 and 7:5:1	Litho contrast/structure/ gneiss	Mwaniki et al. 2015, Pour and Hashim 2015, Joseph and Bamidele 2018, Hamimi et al. 2020

Landsat 5 (TM)	7:4:2, 5:4:3, 7:5:4, 4:5:7, 1:4:7	Litho contrast/ metagabbro/ gneiss/ Clays	Longi et al. 2001, Ali and Pour 2014, Mwaniki et al. 2015, Saibi et al. 2018
(ASTER 1 ASTER 2 ASTER 3)	6:2:1, 7:4:2, 789, 4:6:8, 5:2:1, 6:3:1, 7:4:3, 13:12:10	Litho contrast/ structure, gneiss, marble	Hewson et al. 2015, Hamimi et al. 2020
SENTINEL 2 S2A-T131948 S2A-T130703	4:3:2, 8:4:3, 12:11:2, 8:11:3, 8A:11:2 or 4, 11:4:12, 11:8:4, 11:8:2, 12:8A:3, 11:8A:2	Litho contrast/structure	Mwaniki et al. 2015, Fal et al. 2018, El Atillah et al. 2019
SRTM & AST_ DEM		Litho structures	

Table 2: Multispectral data processing with different band ratios (BR) tested in the course of this study.

Satellite Data	Band Ratios	Target/lithology	References
Landsat 8 (2015 & 2017)	4/2:7/6:5/4, 6/2:7/4:6/3, 4/2:5/6:7/5, 4/2:6/7:5, 4/2:5/3:6/7, 6/4:5/3:4/2, 4/2:6/2:7/3, 4/3:5/2:7/4, 7/1:5/3:4/2, 4/3:6/2:7/4, 4/2:6/7:6/5, 7/6:7/5:5/3	Litho contrast/ structures, Gneiss	Ali and Pour 2014, Pour and Hashim 2015, Mwaniki et al. 2015, Joseph and Bamidele 2018, , Saibi et al. 2018, Asran and Hassan 2021, Hamimi et al. 2020 ,
Landsat 5 (TM)	1/3:5/7:3/5, 5/3:5/1:7/5, 3/2:3/7:4/7, 5/7:3/2:4/5, 5/7:5/1:3/4, 7/5:5/4:3/1, 3/1:4/2:7/5	Litho contrast/ structures/ gneiss	Abdeen et al. 2001, Mshiu 2011, Cudahy 2012,

(ASTER 1 ASTER 2 ASTER 3)	14/12, 13/14, 12/13, (7+9)/8, (5+7)/6, (6+9)/(7+8), (5*7)/6*6, 4/2:4/3:2/1, 4/5:5/6:5/8, 2/1:4/3:5/6, 2/1:4/3:5/8, 4/7:4/3:2/1, 4/7:3/4:2/1, 4/7:5/6:2/1, 5/4:2/1:4/1, 8/5:5/4:8/7	Litho contrast/ structures/ gneiss	Abdeen et al. 2001, Cudahy 2012, CSIRO 2012, , Asran and Hassan 2021, Rezaei et al. 2019
SENTINEL 2A S2A-T131948 S2A-T130703	11/8:11/2:11/12, 11/12:11/2:11/8, 12/4:12/2:11/3 and 12/2:11/2:8/11	Litho contrast/ gneiss	El Atillah et al. 2019

Table 3: Multispectral data transformation, enhancement, and classification techniques tested in this study.

Satellite Data	Enhancement/ Classification method	Target/lithology	References
Landsat 8 OLI 1 (2017) OLI 2 (2015)	PCA 2:4:5, 3:4:5, 5:6:7,1:2:3, 2:3:4, 6:5:4 MNF, DS, SVM, MLC, SAM for band ratio 4/2:7/6:5/4	Litho contrast	Mwaniki et al. 2015, Hamimi et al. 2020, Joseph and Bamidele 2018
Landsat 5	PCA 5:4:3, 2:1:3/3:2:1, MNF 3:2:1	Litho contrast	Pour et al. 2015, Saibi et al. 2018
ASTER 1 ASTER 2 ASTER 3	PCA 3:2:1,1:2:3, 5:4:2, 5:7:9 ICA 2:3:1, 4:6:8, 7:8:9, 4:5:6 SAM, MLC 3:2:1 by ROIs & Spectra	Litho contrast, gneiss, gabbro, serpentinite	El Kati et al. 2018, Arivazhagan and Anbazhagan 2017, Pour et al. 2015
SENTINEL 2 S2A-	DS 4:3:2, PCA 8:11:3 & 11/2:11/2:8/11, Unsupervised	Litho contrast	Fal et al. 2018

T131948 S2A- T130703	classification by K-Means and IsoData		
SRTM & AST_DEM	Shaded relief, & DEM slope images	Structures	JOGMEC

To highlight the discrimination of lithological features, image processing techniques were applied on available multispectral (ASTER, Landsat 5, Landsat 8, and Sentinel 2A) data by band combination (BC), band ratio (BR), and image classifications. In addition, geological mapping was boosted by supervised classification by collected endmember spectra from sampled rocks on Sentinel 2A data and mineral and spectral analyses for rock identification and nomenclature. The results from ASTER data processing are not presented in this article because they were of poor quality, which limited the characterization of geological features.

Results

Landsat TM 5 and Landsat 8 (OLI) Data Analytic Results

The crystalline marble unit have been delineated as linear figures in the northeast and northwest areas using the band combination and band ratio image processing techniques. However, the Landsat (TM5) band combinations (BC) images 3:2:1, 7:4:2, 7:5:4 and band ratio (BR) images 3/2:3/7:4/7, 5/3:5/1:7/5, 7/5:5/4:3/1 failed to produce images that could map different lithologic units because of loss of spectral pixels after image processing procedure of masking of clouds, vegetation cover and the resolution of the data itself. For Landsat 8 data, crystalline marble units could be distinguished from others by the band combination (BC) 7:6:4 and 5:6:7 images and by band ratio (BR) images 4/2:7/6:5/4 and 6/2:7/4:6/3. No other geologic unit was mapped by the processing of Landsat 8 data. Images produced after band combination and band ratio processing of

Landsat 5 and Landsat 8 data are not included in this publication due to their poor quality.

Sentinel 2A Data Analytic Results

The Sentinel 2A multispectral data are preferably used for their relatively high resolution (10 m) on bands 2, 3, 4, and 8, which are resampled with bands 6, 8a, 11, and 12, which have 20 m spatial resolution. Within the VNIR and SWIR region of the electromagnetic spectrum, Sentinel 2A data have higher spatial and spectral resolution than ASTER, Landsat TM5, and Landsat 8 (OLI) data (Fal et al. 2018).

Sentinel 2A data band combination (BC) natural colour image is produced with spectral bands 4:3:2 in Red: green: blue ratio (Figure 3a). Sentinel band combinations BC 12:8A:4 shows vegetation cover in the area in green colour (Figure 2b), whereas image BC 12:11:3 shows potential for demarcation of geological boundaries. Different applied band combinations (BC) and band ratios (BR) tested in tables 1 - 3 are presented in figure 3a - d. Sentinel 2A data band combination (BC) natural colour image is produced with spectral bands 4:3:2 in red: green: blue ratio (Figure 3a). Sentinel 2A data BC 12:8A:4 shows vegetation cover in the area in green colour (Figure 3b), whereas image BC 12:11:3 shows potential for demarcation of geological boundaries (Figure 3c).

In this study, images BC 8:11:3 and BR 12/2:11/2:8/11 and decorrelation stretch (DS) images 4:3:2 and 8:11:3 were selected to demarcate the geological boundaries in the QDS 148 block because of their enhanced image colour contrast (Figure 4a - d).

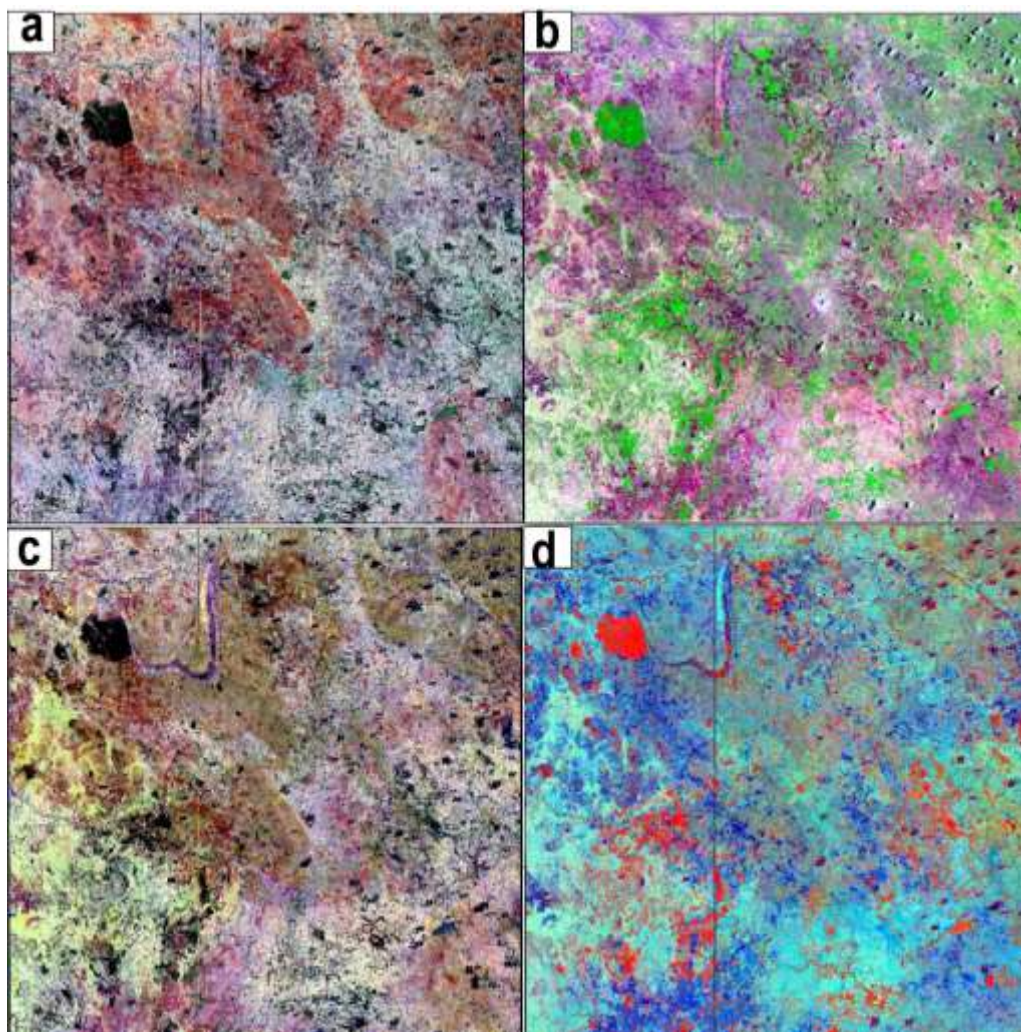


Figure 3: Images from the Sentinel 2A band combination (BC) and band ratio (BR): (a) S 2A BC 4:3:2 (natural colour image) (b) S 2A BC 12:8A:4 image showing vegetation in green (c) S2A BC 12:11:3 image and (d) S 2A BR 11/12:11/2:11/8. Each image represents an area of 55 km length (L) by 55 km width (W) at a scale of 1:300,000.

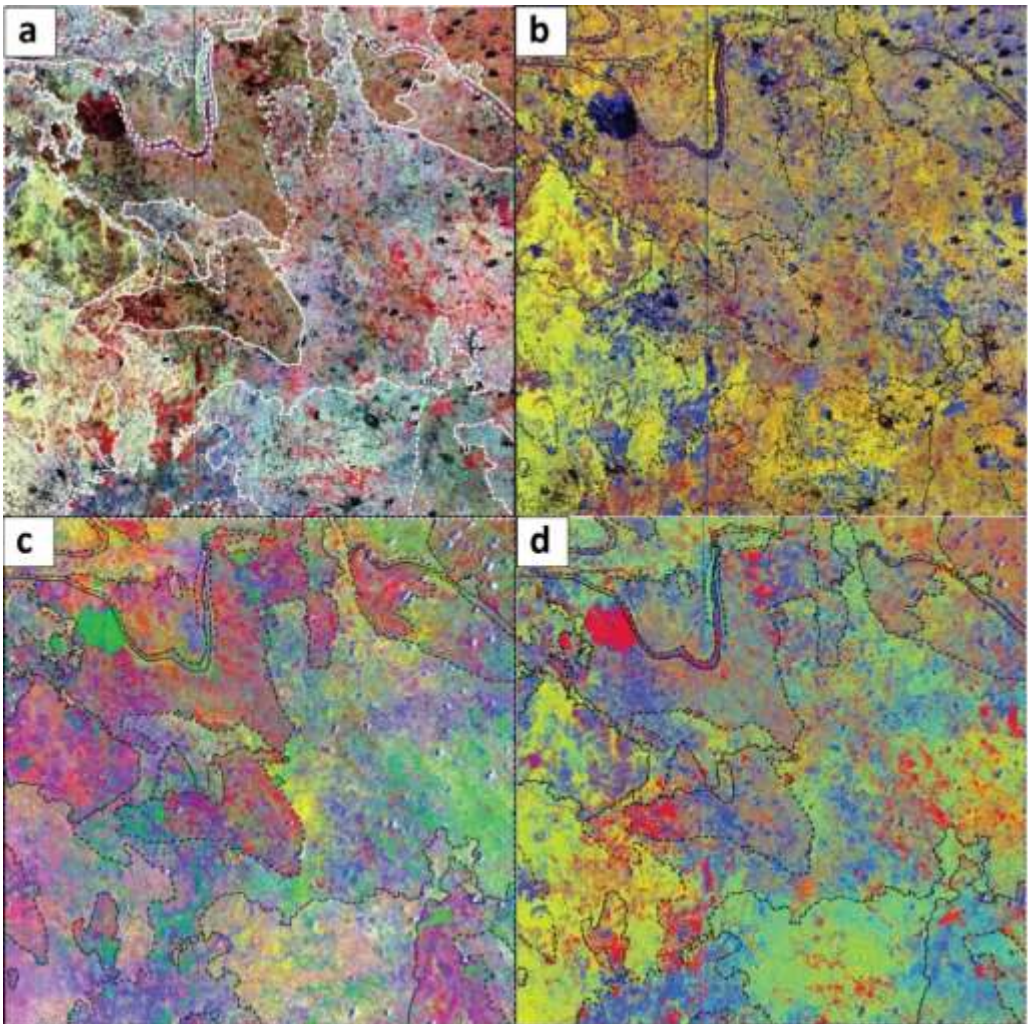


Figure 4: S2A Geologic mapping images with traced geological boundaries in dashed lines: (a) S2A BC 8:11:3 image, (b) S2A BR 12/2:11/2:8/11 image (c) S2A DS 4:3:2 Image and (d) S2A DS 8:11:3 image. Each image represents an area of 55 km length (L) by 55 km width (W) at a scale of 1:300,000.

In addition, image colour-transform techniques, principal component analysis (PCA), and decorrelation stretch (DS) appear to add spectral colour contrast to the composite images. DS 4:3:2 and 8:11:3 and PCA 8:11:3 images added spectral contrast to help demarcate major lithologic boundaries in the study area (Figure 4c and d). Unsupervised classification by Iso-Data and supervised classification by minimum distance

algorithms enabled to map lithologic units (gneisses and granulite) with similar mineral assemblage as one unit. The classification could not distinguish smaller units like meta-gabbro, meta-anorthosites, amphibolite, and pyroxenite from the gneissic units. Therefore, the two classifications produced similar spectral mapped patterns (Figure 5a and b).

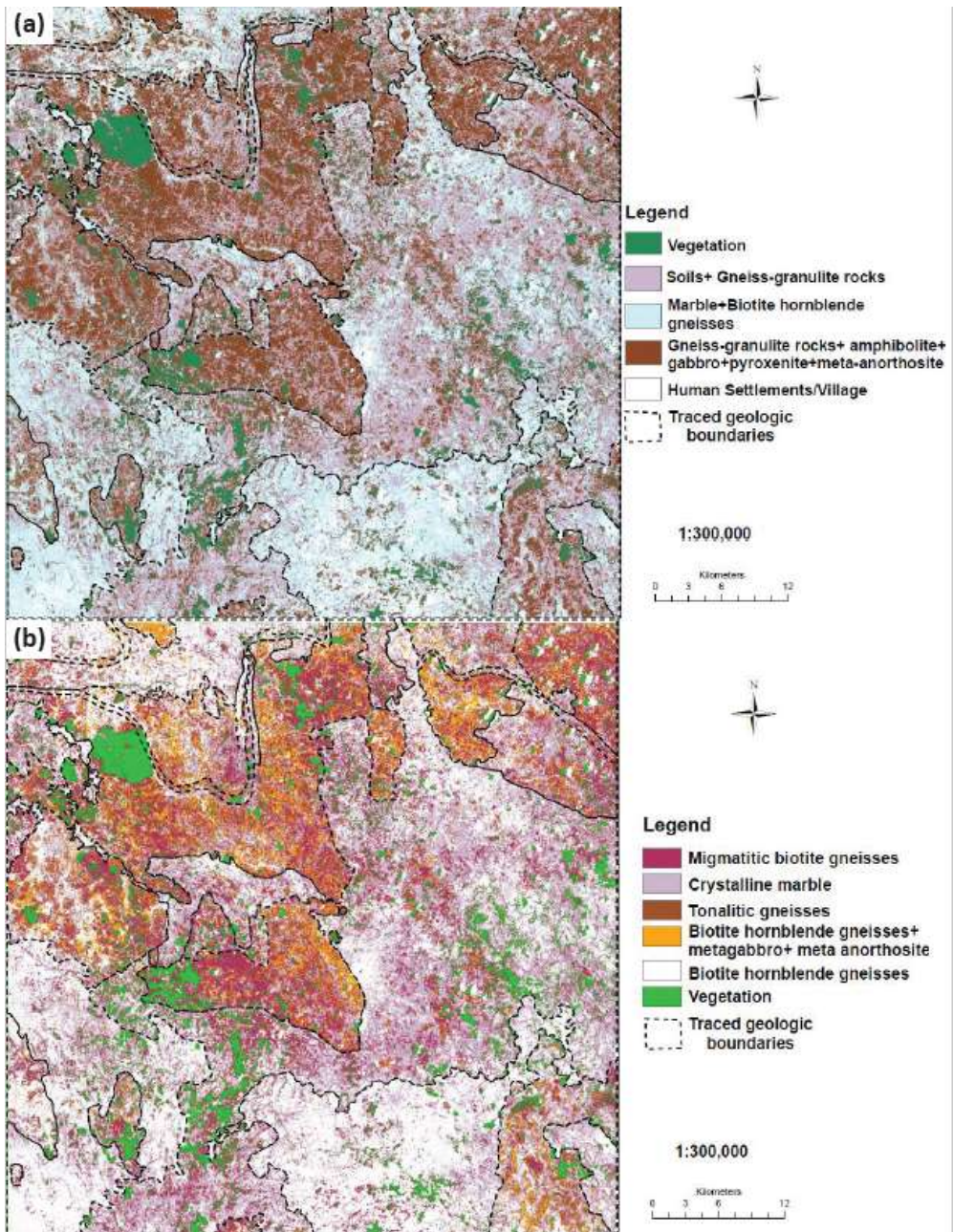


Figure 5: Classification images of Sentinel 2A with traced geologic boundaries: (a) Unsupervised classification image of Sentinel 2A data by Iso-Data algorithm with 5 classes and (b) Supervised classification map of Sentinel 2A data by minimum distance algorithm with 6 classes.

Rock Spectral Results

The analytic results demonstrate that spectral geologic mapping produced a classified image with in-homogeneous pixels delineating major

lithologic unit boundaries pertinent to constituent mineral assemblage. Mineral spectra of interpreted rock-forming minerals were collected from the ENVI spectral analyst

and selected rock spectra from the Handeni (QDS 148) Block were used for spectral analysis. The spectral profile from rock samples of different lithological units collected in the study area have displayed absorption features at wavelengths 1.4, 1.9, 2.2 to 2.31, and 2.38 micrometres (μm) wavelengths (in the SWIR region). Spectral signatures of lithologic units and their respective rock-forming minerals assisted in spectral geologic mapping and identification. The similarity of mineral composition of different rock units complicated the spectral mapping results. Spectral analysis shows that the spectral signals of the rocks are produced mainly by m hornblende, pyroxene, feldspar, and quartz minerals.

Rock spectroscopy from samples and their respective composing minerals have average

spectral features occurring near 1406, 1906, 2119, 2322, and 2380 nanometer (nm) wavelength. This range is within the SWIR region of the electromagnetic spectrum, of which Sentinel 2A data have a higher spectral and spatial resolution; hence, more useful to highlight geological boundaries in QDS 148 Block due to enhanced image colour contrast. Nine (9) rock spectra in the Sentinel 2A data produced classified image (Figure 6) with spectral signatures similar to those obtained during multispectral data processing and enhancement, which complemented the delineation of lithologic boundaries of the Handeni (QDS 148) Block. The representative spectra used were from gneiss, granulite, and crystalline marble units, which cover and represent a large part of the lithologic units mapped in the study area.

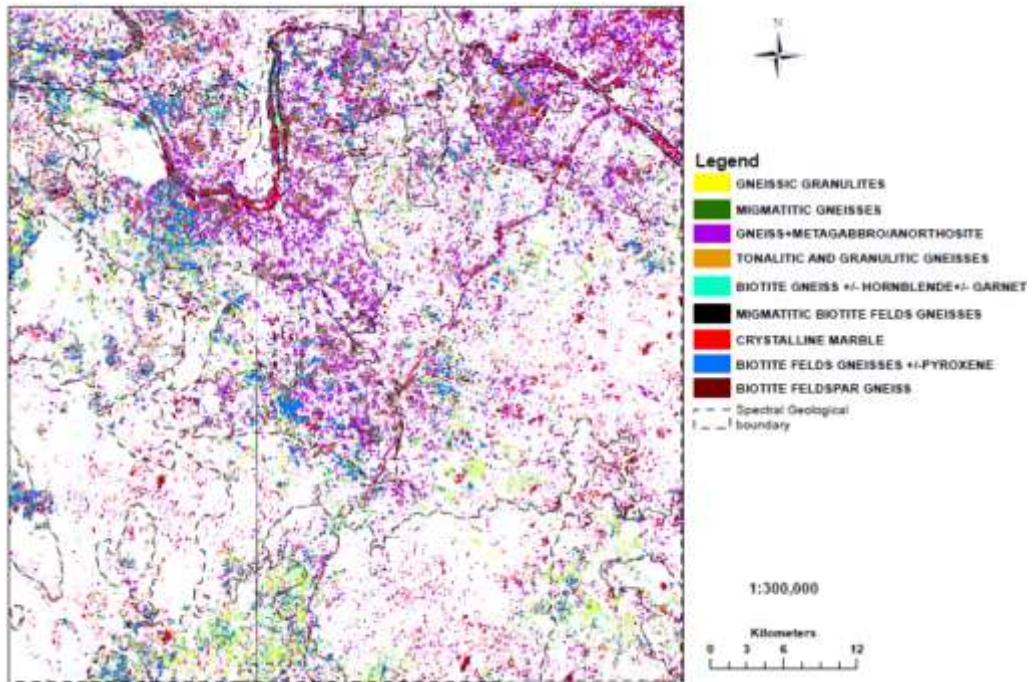


Figure 6: Rock spectral classification map of Sentinel 2A data, showing classified rocks pixels with delineated lithological boundaries in dashed lines.

Mineral Analytic Results

Mineralogic analyses (XRD, TSG, and petrology) of samples have shown that the rocks are composed of plagioclase -

hornblende - pyroxene group of minerals and quartz as major rock-forming constituents, with accessory minerals like biotite, chlorite, siderite, kaolin, and montmorillonite.

Delineation of geologic boundaries was integrated with petrographic and XRD analytical results for the mineralogical and nomenclature of classified lithological units shown in the final map in figure 7. Generally, the geology of the study area dominantly comprises gneiss and granulite as major rock units, with amphibolite, pyroxenite, meta-gabbro, and marble as subordinate lithologies.

Discussion

The processing and analysis of RS multispectral data in this study produced results of images that enabled the delineation of carbonates (crystalline marble and limestone), alluvial deposits, mbuga soils, and gneissic granulite units in the Handeni (QDS 148) Block. However, during the ground field check, marble, gabbro-metagabbro, anorthosite, pyroxenite, amphibolites, felsic to mafic granulites, gneissic rock assemblage and quartz veins units were also mapped. Handeni (QDS 148) Block is characterized by various lithologic units that have almost similar mineral assemblages, with the exception of carbonate rocks. Crystalline marble was mapped with Landsat 8 (OLI) BCs 5:6:7 and 7:6:4 images (e.g., Joseph and Bamidele 2018) and band ratio (BR) images 4/2:7/6:5/4 and 6/2:7/4:6/3. Processing of Sentinel 2A (S2A) data produced BC 8:11:3, BR 12/2:11/2:8/11, 12/4:11/3:11/2, 12/4:12/2:11/3 images that were useful for lithologic mapping by also delineating alluvial deposits, mbuga soils, and gneiss-granulite sequence (e.g., Fal et al. 2018, Mwaniki et al. 2015, El Kati et al. 2018, El Atillah et al. 2019). Unsupervised (IsoData algorithm) and supervised (Minimum distance algorithm) classification images of Sentinel 2A data in figures 5a and b clarified the mapping of major lithologic boundaries. The classified rock spectral resulting image of Sentinel 2A data in figure 6 shows a resemblance with figures 4a

and b, demonstrating that rock spectroscopy can be used to aid in geologic mapping. RS multispectral data processing failed to distinguish lithologic units like gabbro-metagabbro, pyroxenite, anorthosite, amphibolites, and quartz veins units from the gneiss-granulite sequences. ASTER, Landsat (TM5), and OLI 8 data only managed to map carbonates but were ineffective in mapping other geologic units because of the loss of essential pixels after masking due to extensive vegetation and cloud covering the study area and their low spectral resolution of the data also contribute to the observed failure in discriminating all lithologies.

In spectral mapping, gneisses may have different spectral signatures because of variations in the quantity of certain mineral content though they may both contain the same type of minerals. Spectral signatures of gneisses rocks may also be determined by accessory minerals instead of major forming minerals (Longhi et al. 2001). Spectral signatures from representative rock samples were used as endmembers in spectral classification for geologic mapping. The representative rock spectra used were from gneiss, granulites, and crystalline marble units because they were the dominant lithologic units in coverage. However, not all rock spectra were classified as separate distinguished lithologic units because these spectra were collected from rocks with similar mineral compositions/ assemblages. Therefore, they give identical spectral patterns when using remote sensing satellite data during mapping. Even with that challenge, W23 (biotite-hornblende-feldspar gneiss) and WP4 (crystalline marble) were mapped almost similarly to the images that were produced by supervised and unsupervised classification algorithms (Figure 5a and b).

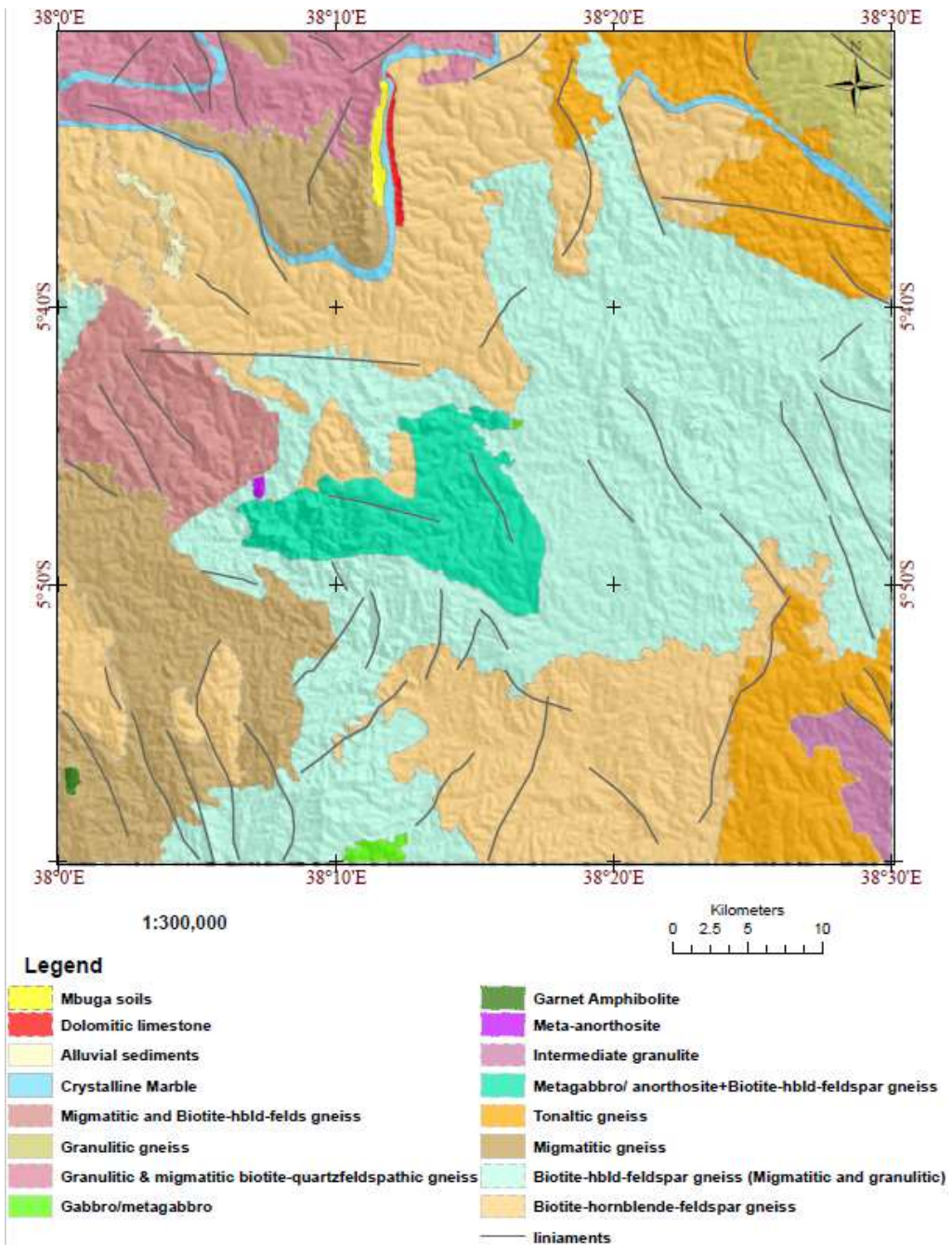


Figure 7: Geological map of Handeni (QDS 148) Block produced in this study. The illustrated geological boundaries digitized after integration of multi-satellite data; XRD and petrographic analyses, and spectral lithologic mapping results.

A synthesis of all RS data processing coupled with multispectral data analytic results, rock spectroscopy, and mineral

analyses results has enabled to successfully map the Handeni (QDS 148) block (Figure 7). The produced map was then compared with

the previous geological maps (Figure 2b) for validation. Ninety-six randomly selected points (samples) were used in the accuracy assessment contingency table to validate the accuracy of mapped geological units produced. The overall accuracy of the assessment is 59%, and the Kappa coefficient of 0.54. This is relatively low accuracy, and Kappa values are attributed mainly to two factors, which are the similarity in mineral composition of the lithologic units in the study area and how they were demarcated in the reference map (Figure 2b) used in the validation process. The similar mineral composition produced the identical spectral signatures used to demarcate geological boundaries created in this study (Figure 7). The reference map (Figure 2b) and assessed map (Figure 7) have been produced from sub-surface (high-resolution radiometric data) and on-surface (spectral) signals, respectively. Validation of the produced map (Figure 7) to a legacy map (Figure 2b) as a reference led to relatively low accuracy indicator values due to interferences of mineralogical and spectral signatures when assessing/ mapping them on each other.

Ultimately, the mapping results indicated that geologic mapping using RS technology has effectively delineated some of the geological boundaries that could have been difficult to trace using conventional mapping techniques due to the remoteness of the terrane and overburden cover (e.g., Fal et al. 2018), which increased the accuracy of the produced surface geologic map (Figure 7).

Conclusions

Remote sensing data and spectroradiometry were used to map the geology of the Handeni (QDS 148) Block in combination with conventional geologic mapping (ground truthing). The results indicate that:

- Landsat 5 (TM) image band ratio 3/1:7/5:5/3 and band combinations 7:5:4 and 7:4:2 delineate marble/limestone unit.
- Landsat 8 (OLI) data, carbonate units were mapped by band combinations 5:6:7 and 7:6:4 and band ratios 6/2:7/4:6/3 and 6/4:5/3:4/2.

- Lineaments have been successfully mapped from ASTER-DEM data.
- Sentinel 2A data proved more useful in the analysis as it mapped marble, limestones, alluvial deposits, and assemblage of gneissic-granulitic units by BC 8:11:3, BR 12/4:11/3:11/2, 11/12:11/2:11/8, and 12/4:12/2:11/3.
- Sentinel 2A data and rock spectral classification images were useful in mapping out major geological units, mainly gneisses.

The map produced by this study also has lithologic boundaries similar to previously reported boundaries where geologic boundaries were digitized following high-resolution radiometric data. In this study, however, some of the lithologic units such as serpentinites, gabbro/ metagabbro, amphibolite, pyroxenite, which occur in gneissic-granulite rocks and superficial materials, were not mapped because of several factors such as their size, type of the multi-spectral data used (Landsat 5, Landsat 8 and ASTER), loss of spectral information due to masking of clouds and vegetation and their respective mineralogical composition of which determine the visibility of their spectral.

The approach is relatively time and resource adequate to supplement conventional geologic mapping, and it is more relevant to areas that are basically unmapped and complex and poorly exposed terranes. Rock spectral analysis and classification can play a significant role in mapping lithologic boundaries of different rock units when used together with multispectral data analysis. The surface of rock units can display diagnostic reflectance spectral signatures controlled mainly by their mineralogical composition, surface freshness (weathering), colour, and texture of constituting materials. The findings of this study have shown that there is a room to expand research in spectral lithologic mapping in other geologic settings to learn more about the outcome of remote sensing in geologic mapping and complement conventional lithologic mapping.

Acknowledgements

The authors are thankful to the Geologic Survey of Tanzania (GST) for providing a bursary for a Master's research study to its staff, the first author, Masota Magigita.

References

- Abdeen M, Thurmond AK, Abdelsalam M, Stern B 2001 Application of ASTER band-ratio images for geological mapping in arid regions; The Neoproterozoic Allaqi Suture, Egypt. *Egypt Geol. Soc. Am.* 33: 289.
- Ali AS and Pour AM 2014 Lithological mapping and hydrothermal alteration using Landsat data: a case study in Ariab mining district, red sea hills, Sudan. *Int. J. Basic Appl. Sci.* 3(3): 199-208.
- Archibald SM 2013 Technical report on the Handeni Property centered at 39.97⁰E, 5.753⁰S Tanga Province, Kilindi district Tanzania NI 43-101.
- Asran MA and Hassan SM 2021 Remote sensing-based geological mapping and petrogenesis of Wadi Khuda Precambrian rocks, South Eastern Desert of Egypt with emphasis on leucogranite. *Egypt. J. Remote Sens. Space Sci.* 24(1) 15-27.
<https://doi.org/10.1016/j.ejrs.2019.07.004>
- Arivazhagan S and Anbazhagan S 2017 ASTER Data Analyses for Lithological Discrimination of Sittampundi Anorthositic Complex, Southern India. *Geosci. Res.* 2(3): 196-209.
- Bhagwat SB and Ipe VC 2000 Economic benefits of detailed geologic mapping to Kentucky Special Report 3, Illinois State of Geological Survey, Illinois.
- Bhan SK and Krishnanunn K 1983 Applications of remote sensing techniques to geology. *Indian Acad. Sci. (Eng.. Sci.)* 6, Pt.4: 297-311.
- Chao DJ 1974 Brief explanation of the geology, QDS 148. GST unpublished report.
- Chunming Wu, Xiao Li, Weitao Chen, Xianju Li 2018 A review of geological applications of high-spatial-resolution remote sensing data.
- Cudahy T 2012 Satellite ASTER Geoscience Product Notes for Australia, *Version 1, CSIRO ePublish* No. EP-30-07-12-44.
- El Kati I, Nakhcha C, El Bakhchouch O and Tabyaoui H 2018 Application of Aster and Sentinel- 2A Images for Geological Mapping in Arid Regions: The Safsafate Area in the Neogen Guercif basin, Northern Morocco. *International J. Adv. Remote Sens. GIS* 7(1) 2782-2792.
- El Atillah A, El Morjani ZEA and Souhassou M 2019 Use of the Sentinel-2A multispectral image for litho-structural and alteration mapping in Al Glo'a map sheet (1/50,000) (Bou Azzer-El Graara Inlier, Central Anti-Atlas, Morocco). *Artif. Satel.* 54(3)
- Fal S, Maanan M, Baïdder L, and Rhinane H 2018 The contribution of Sentinel-2 satellite images for geological mapping in the south of Tafilalet basin (Eastern Anti-Atlas, Morocco). *Int. Arch. Photogramm. Remote Sens. Spatial Inf. Sci.* doi.org/10.5194/isprs-archives-XLII-4-W12-75-2019
- Gandhi SM and Sarkar BC 2016 Essentials of Mineral Exploration and Evaluation Elsevier Inc. GST 2018 Tanzania Mapping Progress Map (*Unpublished map*).
- Hamimi Z, Hagag W, Kamh S and El-Araby A 2020 Application of remote-sensing techniques in geological and structural mapping of Atalla Shear Zone and Environs, Central Eastern Desert, Egypt. *Arab. J. Geosci.* 13: 414.
- Hewson R, Robson D, Mauger A, Cudahy T, Thomas M and Jones S 2015 Using the Geoscience Australia-CSIRO ASTER maps and airborne geophysics to explore Australian geoscience, *J. Spat. Sci.* 60(2) 207-231.
- Joseph A and Bamidele, O 2018 Application of Remote Sensing Method for Geological Interpretation of Sokoto Plain, Nigeria. *South Afr. J. Geomat., Vol. 7. No. 3.*
- Leger C, Barth A, Knobloch A, Mruma AH, Myumbilwa Y, Magigita M, Msechu M,

- Ngole T, Stanek KP 2015 Minerogenic Map of Tanzania 1:1,500,000, GST published Map.
- Longhi I, Sgavetti M, Chiari R, Mazzoli C 2001 Spectral analysis and classification of metamorphic rocks from laboratory reflectance spectra in the 0.4-2.5 Um interval: A tool for hyperspectral data interpretation. *Int. J. Remote Sens.* 22(18): 3763- 3782.
- Maswi MS and Mshiu EE 2020 Delineation of Geothermal Potential Sites Using Remote Sensing Satellite Data-Lake Natron, Northern Tanzania. 8th African Rift Geothermal Conference 2-8 November 2020.
- Moses F, Bazil MP, Nyanda P, Macheyeke AS, Bushi A, Baglow H, Grantham GH, Thomas RJ, Jacobs J 2015 Explanatory notes of the geology of the Handeni block (QDS 146-148 and 166-167) in Eastern Tanzania (Scale 1: 100000), GST published report.
- Mshiu EE 2011 Landsat Remote Sensing Data as an alternative approach for geological mapping in Tanzania: A case study in the Rungwe volcanic province, Southwest Tanzania. *Tanz. J. Sci.* 37: 26-36.
- Mwaniki MW, Moeller MS and Schellmann G 2015 A comparison of Landsat 8 (OLI) and Landsat 7 (ETM+) in mapping geology and visualizing lineaments: A case study of central region Kenya. *The International Archives of the Photogrammetry, Remote Sensing and Spatial Information Sciences, 36th International Symposium On Remote Sensing of Environment*, 11–15 May 2015, Berlin, Germany. Volume XL-7/W3: 897-903.
- Pour AM, Hashim M and Pournamdari M 2015 Chromitite prospecting using landsat TM and ASTER remote sensing data. *ISPRS Ann. Photogram, Remote Sens. Spat. Inform. Sci.* Volume II-2/W2.
- Rezaei A, Hassani H, Moarefvand P and Golmohammadi, A 2019 Lithological mapping in Sangan region in Northeast Iran using ASTER satellite data and image processing methods. *Geol. Ecol. Landscapes*, 4 (1) 59-70.
- Rao AD, Guha A, Kumar VK and Rao DEN 2017 Potentials of Spectrometry in Economic Rocks Mapping -A Brief Analysis for Three Economic Rocks of Three Different Geological Provinces of India. *J. Remote Sens. GIS* 6: 218.
- Saibi H, Bersi, M, Mia MB, Saadi NM, Al Bloushi KMS and Avakian RW 2018 *Applicat. remote Sens. Geosci.* 9:181-203.
- Solesbury FW 1964 Brief explanation of the geology, QDS 148. GST unpublished report.
- Soller DR 2004 *Introduction to Geologic Mapping*, McGraw-Hill Yearbook of Science & Technology U.S. Geological Survey 128-130.
- Yajima T, Kawakami Y, Mityatake S, Hayashi T, Kadowaki N, Deguchi T and Kawai M 2009 Geological mapping in the vegetated terrain sing polarimetric synthetic aperture radar data. *The Asian Conference on Remote Sensing, Vol. 30th Beijing, October 2009.*